

# $H_\alpha$ Imaging of Solar Phenomena Using a Modified Schmidt-Cassegrain Telescope at Astronomical Observatory - Belogradchik

Pencho Markishki<sup>1</sup>, Momchil Dechev<sup>1</sup>, Werner Pötzi<sup>2</sup>, Rositsa Miteva<sup>1</sup>,  
Kamen Kozarev<sup>1</sup>

<sup>1</sup> Institute of Astronomy and National Astronomical Observatory, Bulgarian Academy of Sciences, BG-1784, Sofia

<sup>2</sup> Institute of Physics, Kanzelhöhe Observatory for Solar and Environmental Research, University of Graz, 8010 Graz, Austria  
mdechev@astro.bas.bg

(Submitted on 29.05.2025; Accepted on 17.06.2025)

**Abstract.** This paper presents the technical setup and observational results of a solar imaging system deployed at the Astronomical Observatory Belogradchik (AO-Belogradchik). A Celestron C11 Schmidt-Cassegrain telescope, equipped with a DayStar Energy Rejection Filter (ERF) and a Hydrogen Alpha ( $H_\alpha$ ) Quantum filter, was used to capture high-resolution images of solar prominences and sunspots. The optical configuration of the system, including the optimization of the focal ratio (f/31.1) and thermal stabilization, enabled precise  $H_\alpha$  imaging. Angular-resolution calculations (1.83") and linear-resolution (24.9  $\mu\text{m}$ ) confirmed the capability of the system to resolve fine solar features. The results demonstrate the effectiveness of off-axis ERF mounting and pixel binning for CMOS sensor optimization.

**Key words:** Solar observations, Prominences, Flares, Belogradchik observatory

## 1 Introduction

Solar activity phenomena arise from the intrinsic magnetism of our star, generated by the dynamo process (currently assumed to be in the so-called Tychocline) and convective motions helping the magnetic field bundles to migrate [Christensen-Dalsgaard, 2021]. Historically, solar activity has first been observed as dark spots on the visible surface, termed sunspots [Arlt and Vaquero, 2020]. Nowadays it is well known that they are areas of highly concentrated magnetic field lines (up to about 3000 Gauss), thus impeding the heat transfer leading to their darker appearance (the temperature in the umbra (central part) could be as low as half of the quiet photosphere). Nowadays, the sunspots are routinely observed in white light, and their daily reports are used to calculate the solar cycle [Hathaway, 2015], e.g. <https://www.sidc.be/SILSO/home>. The area containing the sunspots is known as an active region (AR) comprising a variety of solar features [van Driel-Gesztelyi and Green, 2015].

In visible light, during total solar eclipses or coronagraph observations, bright loops can be seen at the solar limb, known as prominences, whereas when viewed in projection on the solar disk (using narrow-band filters), they appear dark and are known as filaments [Gibson, 2018]. The prominences are cooler than their environment and consist of plasma structures that are often suspended in the solar corona. Occasionally, their balance is compromised, and the plasma erupts in the interplanetary (IP) space.

The most energetic explosions in the solar atmosphere are known as solar flares (SFs) [Benz, 2017], since they appear as intense and short-lived brightening on solar images. SFs are not only electromagnetic (EM) emission, but also involve major rearrangements of the magnetic field line configuration in the ARs, mass motions, and particle accelerations.

Apart from white-light emission, the Sun is monitored over the entire EM spectrum as well. Ground-based observations are possible in visible, infrared, and radio wavelengths, though with partial UT-coverage. The high-energy observations are possible from space only, due to the protection of the terrestrial atmosphere. When dedicated spacecraft are available, they offer uninterrupted solar monitoring. Each wavelength probes different layers from the solar atmosphere, and thus can 'see' different solar phenomena. In this study, we focus on the (red end of the) visible spectrum.

Solar observations in the  $H_\alpha$  wavelength (6562.8 Å) provide critical insights into dynamic phenomena such as prominences, SFs, and ARs (sunspots). However, such imaging requires specialized filters and precise optical configurations to mitigate thermal load and atmospheric dispersion.

Astronomical Observatory (AO)-Belogradchik is located in Northwest Bulgaria, benefiting from a favorable microclimate. Weather data sourced from WeatherSpark<sup>3</sup> indicate a clear season that stretches approximately from early June to late September, with average cloud coverage below 20%. These conditions are suitable for sustained daytime solar observations.

This study details the adaptation of a Celestron C11 telescope at AO-Belogradchik for high-resolution  $H_\alpha$  solar imaging, emphasizing the integration of energy rejection filters, thermal management, and CMOS sensor optimization. Furthermore, we showcase selected test observations made also in different seasonal conditions.

## 2 System Configuration

### 2.1 Telescope

For the purpose of solar monitoring we use Celestron C11 Schmidt-Cassegrain SC 279/2800 C11 Optical Tube Assembly (OTA)<sup>4</sup> (Fig. 1). The technical parameters of the telescope are shown in Table 1.

Parameter	Value
Aperture (mm)	279
Focal length (mm)	2800
Aperture ratio (f/)	10
Tube length (mm)	610
Tube weight (kg)	12.5

**Table 1.** Celestron C11 Schmidt-Cassegrain Parameters

An advanced VX AVX GoTo<sup>5</sup> equatorial mount for stable tracking was used as the mounting. The system is located in the dome of AO-Belogradchik.

<sup>3</sup> <https://weatherspark.com/countries/BG>

<sup>4</sup> <https://www.celestron.com/collections/schmidt-cassegrain-optical-tubes-and-telescopes>

<sup>5</sup> <https://www.astroshop.eu/equatorial-with-goto/celestron-mount-advanced-vx-avx-goto/p,32955#>



**Fig. 1.** Telescope and rejection filter used for the solar observations in AO-Belogradchik.

## 2.2 Filters

For solar observations we need at least one filter to reduce the light and temperature load. For this, the aperture is protected using a rejection/ERF filter, DayStar E-325F90<sup>6</sup> (90 mm diameter), mounted off the optical axis of the telescope (i.e., off-axis) to avoid central obstruction, see Fig. 1. The filter blocks wavelengths  $< 500$  nm and infrared radiation, reducing thermal stress on downstream components.

The ERF filter efficiency is achieved in terms of the following:

- Off-axis mounting: Minimized vignetting and thermal load, critical for prolonged observations
- Sensor Optimization: Binning improved the dynamic range without sacrificing spatial detail
- Comparative Analysis: Resolution metrics align with theoretical predictions, validating the system design.

The second filter which we used for the first test observations is a DayStar Hydrogen Alpha Quantum<sup>7</sup>  $H_{\alpha}$  filter with the following parameters:  $1.25''$ , FWHM  $< 0.5 \text{ \AA}$ , thermally stabilized for spectral consistency. The filter is mounted behind the telescope; see Fig. 2.

<sup>6</sup> <https://www.astroshop.eu/mounted-glass-filters/daystar-filters-energy-rejection-filter-e-325f90/p,52642>

<sup>7</sup> <https://www.daystarfilters.com/quantum/>



**Fig. 2.** Filter and camera system used for the solar observations in AO-Belogradchik.

<b>Parameter</b>	<b>Value</b>
Sensor	Sony IMX304
Light Spectrum	Visible + NIR
Resolution	12.4 MP
Resolution WxH	4112 x 3008 px
Frame rate	23 fps
Cell Size WxH	3.45 x 3.45 $\mu\text{m}$
Weight	130 g
Video Output	8/10/12-bit
Operating Temperature	-5°C to +45°C

**Table 2.** Camera parameters

### 2.3 Camera

The camera used is Common Vision Spark Series, SP-12401M-USB<sup>8</sup>. The camera parameters are shown in Table 2 and can be also seen in Fig. 2.

The pixel size is  $3.45 \times 3.45 \mu\text{m}$  (289.8 px/mm), and the sensor's active area measures  $14.19 \times 10.38 \text{ mm}$ , covering  $147.2 \text{ mm}^2$ . The camera operates at a frame rate of 23.4 fps with 8-, 10-, or 12-bit monochrome output via USB3. The maximum exposure time during operation is  $1/23.4 \text{ s}$  ( $0.042735 \text{ s}$  or  $42735 \mu\text{s}$ ).

<sup>8</sup> <https://www.jai.com/products/sp-12401m-usb>

### 3 Optical Performance Analysis

The configured system has a focal ratio of  $f/31.1$ , which aligns well with the  $H_\alpha$  filter's requirement for a light cone convergence of approximately  $f/30$ . The telescope-camera system's field of view is  $0.290^\circ \times 0.212^\circ$  ( $17.42' \times 12.74'$ ), with an angular resolution of  $0.25''/\text{px}$ .

The angular resolution  $\theta$  of the optical system, according to the Rayleigh criterion, is:

$$\theta = 1.22 \frac{\lambda}{D}$$

where  $\lambda$  is the wavelength of the  $H_\alpha$  red hydrogen line (656.28 nm) and  $D = 90$  mm is the aperture of the ERF filter mounted in front of the objective. Substituting these values,  $\theta = 1.83''$ .

The linear resolution  $\rho$  [ $\mu\text{m}$ ] of the telescope-camera system is:

$$\rho = 1.22 \times \lambda \times \frac{f}{D} = 1.22 \times 0.65628 \mu\text{m} \times 31.1 = 24.9 \mu\text{m}.$$

This corresponds to approximately 40.2 lines per millimeter (1/mm), which is about 7.2 times lower than the camera's sensor resolution (289.8 px/mm). This indicates that pixel binning can be applied.

The above results are calculated based on the Rayleigh criterion, but the fact that objects on the solar surface are planar – have visible sizes, shapes and boundaries, should actually contribute to improving the detail of the images due to the effect of the Edge spread function (ESP).

In addition to the concept of Point spread function (PSF) through a given optical system, there is also an ESF. The latter has an effect in cases where the observed light sources are not point-like (stars), are observed, but objects of visible size, showing details with edges – with some contours. Typical cases are observations of lunar craters and mountains, planetary and terrestrial observations. It is logical to expect that the ESF will also contribute to observations of objects on the solar surface. Under these conditions, the diffraction limit resolution increases noticeably. In the indicated cases, the diffraction limit resolution varies significantly depending on the shape of the observed details. For example, the image of a dark line on a light background is the result of the conjunction of the diffraction images of the two bright adjacent edges, determining the width of the line.

## 4 Results

### 4.1 Sunspots

Observations in white light were made on 2024-10-14 using a Baader 70 mm metal-coated foil as an initial rejection filter. Although not reliable for science-ready output, the high-contrast images revealed umbra-penumbra differentiation; see Fig. 3. For comparison, the same ARs (13852 and 13854) can be inspected at <https://solarmonitor.org/> obtained by the instruments on board SDO. Both sunspot configurations are reported as  $\beta-\gamma$  of the Hale-type sunspot configuration (<https://www.stce.be/educational/classificati> on or <https://www.spaceweather.com/glossary/magneticclasses.html>).

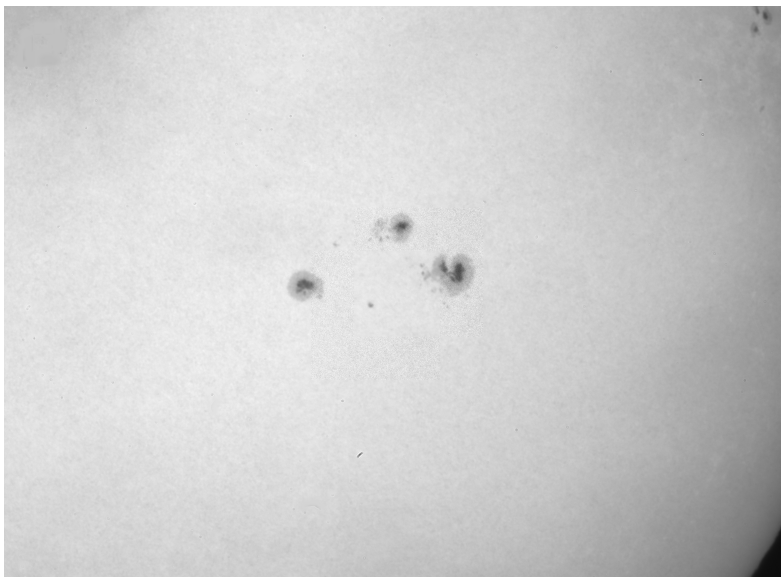


**Fig. 3.** White-light image of the sunspot groups observed on 2024-10-14 at 10:47 UT from AO-Belogradchik (exposure time 14 ms).



**Fig. 4.**  $H_{\alpha}$  images of a prominence in a close succession, observed from AO-Belogradchik on 2024-10-14 at 08:38 UT (exposure time 42 ms each).

## 4.2 Prominences

Filamentary structures were captured in  $H_{\alpha}$  on 2024-10-14, see Fig. 4, showcasing dynamic plasma motions when followed in subsequent images. The solar disk was overexposed in order to highlight the faint prominence structure above the limb.

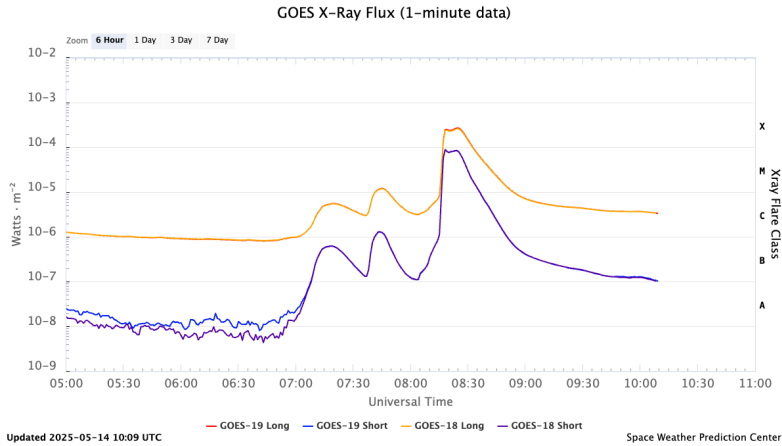


**Fig. 5.** Light curve from GOES on 2025-05-14. Source: <https://www.swpc.noaa.gov/>.

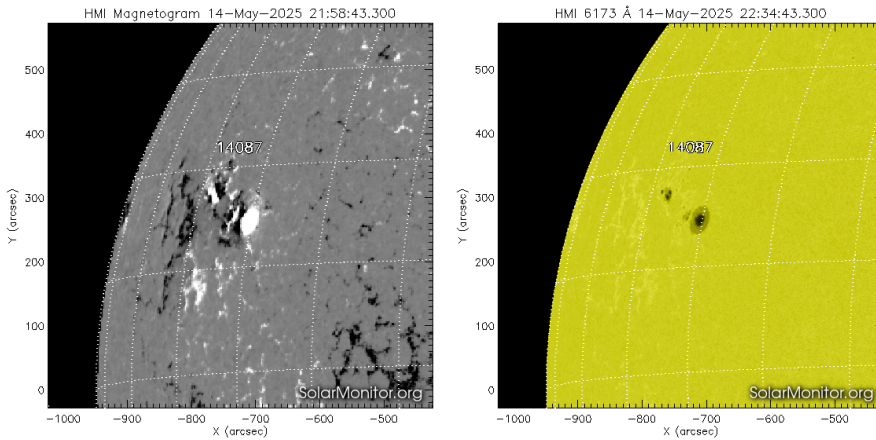


**Fig. 6.** The East-North part of the solar disk on 2025-05-14. Left: SDO/HMI magnetogram, Right: SDO/HMI 6173 Å. Source: <https://solarmonitor.org/>.

### 4.3 Solar flares

Test observations were performed on 2025-05-14 at the time when an X2.7 flare took place. The GOES flux started to increase at 08:04, peaked at 08:25 and ended at 08:31 UT, see Fig. 5. The event originated at N15E68, AR 14087, according to <ftp://ftp.swpc.noaa.gov/pub/warehouse/>. The AR magnetogram and 6173 Å image are shown in Fig. 6 based on SDO data.

The event was recorded by our system. Several  $H_{\alpha}$  frames during the X2.7 SF were manually saved. An example with a superimposed grid is given in Fig. 7. It shows well the sunspot umbra and penumbra, as well as the stric-

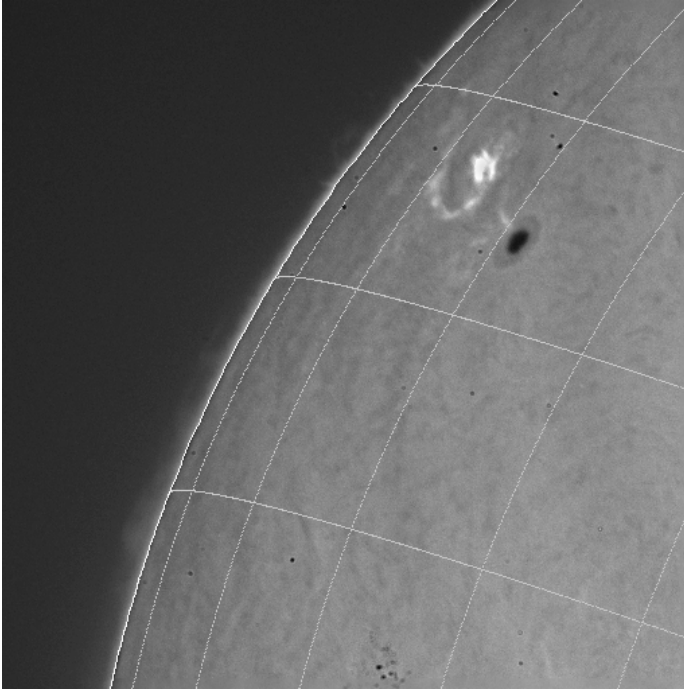


**Fig. 7.**  $H_{\alpha}$  image of the X2-class SF observed on 2025-05-14 (AR 14087) in AO-Belogradchik.

ture of the  $H_{\alpha}$  brightening. Some artifacts from the imaging system are also noticeable. A movie depicting the evolution of the SF is provided as online material.

About 50  $H_{\alpha}$  images were grabbed manually and stored as simple 8-bit images. The first image was recorded at 08:15 UT, whereas the last image – at 08:43 UT. From these images we were able to determine the solar radius and position of the solar disc center. The radius of the solar disc was about 4060 pixels, which corresponds to a resolution of 4.25 pixel per arcsec (or 170 km) on the Sun. With this information a first estimation of the optical flare area could be done, as shown in Fig. 8, where the time axis is only an approximation as the image files did not contain the exact time stamp, and the area is obtained by setting a threshold. The area corresponds to an importance class 1, which is smaller than expected for this type of flare, but due to the low image depth of only 8 bits, the area calculation is also only an approximation.

## 5 Conclusion

The modified Celestron C11 system at AO-Belogradchik demonstrates robust performance in  $H_{\alpha}$  solar imaging, achieving sub-arcsecond resolution and high thermal stability. Successful test observations were performed with a white-light and an  $H_{\alpha}$  filters. The internal structure of sunspots can be recorded

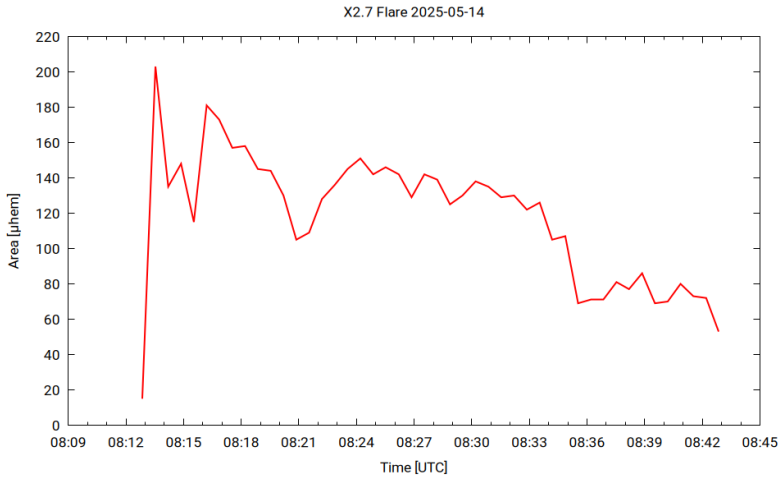


**Fig. 8.** The area of the optical flare in  $H\alpha$  observed on 2025-05-14 at AO-Belogradchik. The area is given in millionths of the solar hemisphere, the time axis is only an approximation as the exact time information was not stored.

in great precision. The procedure of lucky imaging can be applied to detect the flaring structure. The least resolved in all tests were the prominences, however more test observations will be made with the newly obtained Lunt  $H\alpha$  filter. Future applications include real-time monitoring of solar activity and coordinated observing campaigns with other ground-based observatories.

## Acknowledgment

This research was funded by the Bulgarian National Science Foundation project No. KP-06-Austria/5 (14-08-2023) and Austria's Agency for Education and Internationalisation (OeAD) project No. BG 04/2023.

## References

- Arlt, R. and Vaquero, J. M. (2020). Historical sunspot records. *Living Reviews in Solar Physics*, 17(1):1.
- Benz, A. O. (2017). Flare Observations. *Living Reviews in Solar Physics*, 14(1):2.
- Christensen-Dalsgaard, J. (2021). Solar structure and evolution. *Living Reviews in Solar Physics*, 18(1):2.
- Gibson, S. E. (2018). Solar prominences: theory and models. Fleshing out the magnetic skeleton. *Living Reviews in Solar Physics*, 15(1):7.
- Hathaway, D. H. (2015). The Solar Cycle. *Living Reviews in Solar Physics*, 12(1):4.
- van Driel-Gesztelyi, L. and Green, L. M. (2015). Evolution of Active Regions. *Living Reviews in Solar Physics*, 12(1):1.